REVIEW ARTICLE

Understanding droplet jetting on varying substrate for biological applications

Jia Min Lee[1]*, Xi Huang[1], Guo Liang Goh[2], Tuan Tran[1,2], Wai Yee Yeong[1,2]

[1]HP-NTU Digital Manufacturing Corp Lab, School of Mechanical & Aerospace Engineering, Nanyang Technological University, Singapore

[2]Singapore Centre for 3D Printing, School of Mechanical & Aerospace Engineering, Nanyang Technological University, Singapore

(This article belongs to the *Special Issue: Related to 3D printing technology and materials*)

Abstract

In the inkjet printing process, the droplet experience two phases, namely the jetting and the impacting phases. In this review article, we aim to understand the physics of a jetted ink, which begins during the droplet formation process. Following which, we highlight the different impacts during which the droplet lands on varying substrates such as solid, liquid, and less commonly known viscoelastic material. Next, the article states important process-specific considerations in determining the success of inkjet bioprinted constructs. Techniques to reduce cell deformation throughout the inkjet printing process are highlighted. Modifying postimpact events, such as spreading, evaporation, and absorption, improves cell viability of printed droplet. Last, applications that leverage on the advantage of pixelation in inkjet printing technology have been shown for drug screening and cell–material interaction studies. It is noteworthy that inkjet bioprinting technology has been integrated with other processing technologies to improve the structural integrity and biofunctionality of bioprinted construct.

Keywords: Inkjet printing; Material jetting; Bioprinting; Additive manufacturing; Hydrogel; Functional material

*Corresponding author:
Jia Min Lee
(jm.lee@ntu.edu.sg)

1. Introduction

Three common material processing technologies have been developed for bioprinting of engineered tissue for biological applications[1-9]. These technologies are material extrusion, material jetting, and vat polymerization printing (VPP). Material extrusion is a technique that dispenses materials through a nozzle using either a pneumatic[10-21] or a mechanical pump[22,23]. Material jetting, a technique which dispenses droplets of material, has variation in the actuation module, such that material is expelled either by a vibrating piezo crystal (as in piezoelectric inkjet printer) or based on vaporized volume of fluid (as in thermal inkjet printer)[24-29]. Alternatively, in the process of laser-induced forward transfer (LIFT), a pulsed laser source directs heat onto a coated quartz ribbon, which causes displacement of microdroplets onto a receiving substrate[30-33]. Last, the process of VPP is characterized by a photopolymer-filled tank that contains cell suspension. The cell-laden photopolymer is later selectively cured to form 3D structures[34-40].
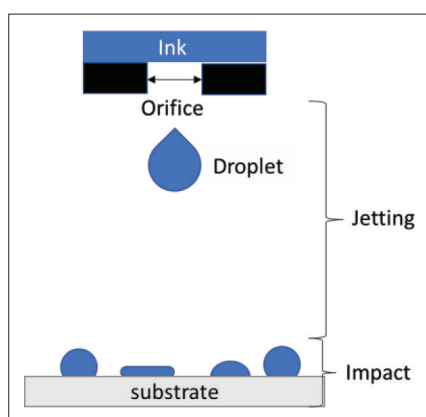
Figure 1. The process of material jetting can be studied at two phases, i.e., jetting and impacting.

The droplet-based bioprinting approach is gaining attention with its advantages, such as contactless and drop-on-demand printing. Moreover, material jetting enables precise control over the deposition pattern and material volume[24,25,41]. Understanding the physics behind inkjet printing processes is beneficial to leverage on the advantages of jetting processes for biological applications. This article discusses the process of inkjet droplet-based printing at two phases, jetting and impacting (Figure 1). The impact phase is further separated into nonpenetrative impact, such as interaction with a solid substrate; and penetrative droplet impact, such as interaction with a liquid pool. A key aspect of this article is to discuss the effect of hydrogel semi-solid substrates on the impact phase. Last, we discuss the use of jetting processes in applications that involve immobilized biomolecules, cell-based assays, and needleless drug delivery system.

2. Droplet formation

Both Newtonian and non-Newtonian fluids with the right fluid properties for jetting may be used in inkjet bioprinting. For inkjet bioprinting, composite microcapsules with a relatively high solids content can also be developed[42]. Therefore, it is crucial to understand droplet formation of both fluid types.

The dimensionless number, Z, is used to describe droplet formation during the jetting phase. Z, which is the inverse of the Ohnesorge number, is used to assess the stability of drop formation[43]. *Oh* is the ratio between the Reynolds and Weber number. The balance between surface energy and viscous dissipation determines how droplets form. For Newtonian liquids, dimensionless numbers such as Reynolds number ($Re = \frac{\rho DV}{\eta}$ ratio of inertial to viscous forces), Weber number ($We = \frac{\rho DV^2}{\sigma}$, ratio of kinetic energy to surface energy) and Ohnesorge number ($Oh = \frac{We^{\frac{1}{2}}}{Re}$) are

useful for describing droplet formation and jet behavior. Droplet with range values of $2 < We_j < 25$ forms stable jet formation. Capillary forces inhibit drop ejection at the lower range, whereas the onset of satellite drop production is indicated above the range. Satellite droplets are artifacts formed due to Rayleigh instability. These artifacts negatively impact printing resolution.

The printability of inks for droplet-based printing, such as inkjet printing, is determined by a dimensionless Z value. Z value captures the relative magnitudes of inertial, viscous, and capillary effects of free-surface fluid mechanics[44]. The minimum velocity for drop ejection is determined by the minimum energy required to overcome surface tension at the nozzle tip ($v_{min} = \left(\frac{4.\sigma}{\rho.d}\right)^{1/2}$)[45].

Deborah number ($De = \frac{\lambda}{t_p}$, where t_p is the time for observation) describes viscoelasticity of a fluid. The t_p depends on the Ohnesorge number of the fluid[46]. If the inertial effect is dominant (Oh < 1), the time for observation is Rayleigh timescale ($t_c = \sqrt{\frac{\rho D^3}{\sigma}}$). If the viscous effect is dominant (Oh > 1), the visco-capillary time scale ($t_v = \frac{\eta D}{\sigma}$) is used instead. While the Deborah number and Weissenberg number are often used interchangeably, they are not the same parameter[47].

The formation of viscoelastic droplet from inkjet printing can be categorized into three types depending on the viscoelasticity of the fluid[48] (Figure 2). At low viscoelasticity, the fluid behaves closer to a Newtonian fluid. When the Deborah number is increased, satellite droplets will form due to Rayleigh instability. By continuing to increase the viscoelasticity of the fluid, the droplet will form a tail when ejected, which at optimal viscoelasticity it will merge back into the droplet. Further increasing the Deborah number will result in satellite droplet again, and at some point, the droplet will not be ejected, and a pullback effect will happen.

During the jetting phase, the main objective is to control and reduce satellite droplet formation. Hardware modification such as having a superhydrophobic sieve is an approach to create a satellite-free single droplet for printing[49]. Another approach is to change the rheology of ink through adding polymers such that drops can remain connected by thin threads during the jetting phase[50-52]. Inertial, capillary, viscous and viscoelastic forces result in generation of droplet from viscoelastic fluid. Weissenberg number $Wi = \frac{\lambda V}{D}$ incorporates the fluid's characteristic relaxation time of fluid, λ, to account for the viscoelastic behavior of non-Newtonian fluids. Polymer relaxation time is a function of molecular weight and polymer concentration. The elastic effects from polymers
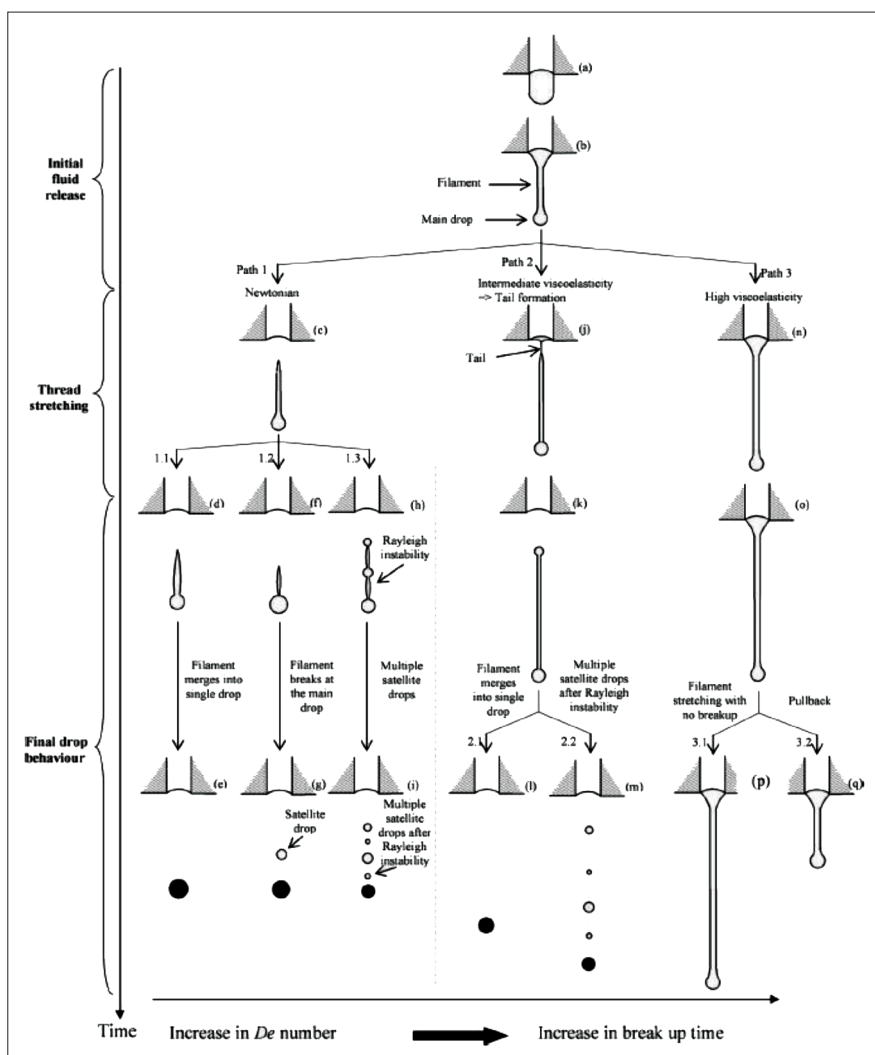
Figure 2. Schematic for droplet formation from inkjet with respect to viscoelasticity of the fluid. (a) and (b) are the ejection and stretching of the droplets which is common to all fluids. (c) to (i) is the breakup of droplet from Newtonian fluid. (j) to (m) is non-Newtonian fluid with intermediate viscoelasticity. (n) to (q) is non-Newtonian fluid with high viscoelasticity. Reprinted with permission from [49]. Copyright (2010), The Society of Rheology.

significantly affect filament thinning, break-up time, and droplet speed, hence minimizing formation of satellite droplets[53]. A bioink with a slow filament elongation and long rupture time has slower droplet velocity[54].

Pneumatic systems are used in microvalve bioprinting to make it easier to print materials with higher viscosity so that tear-off speed for droplet formation can be reached[55]. In other jetting system setup, such as the nozzle-free LIFT, the vapor bubble dynamic is influenced by rheological characteristics, such as surface tension and viscosity[31-33]. The vaporization rate is slower for a substance with higher viscosity, thus reduces the jet velocity.

The droplet enters the impact phase upon interaction with receiving substrate. Droplet impact on solid and liquid substrates has been well studied and the phenomena can be broadly categorized based on the two types of substrates above. Droplets striking solid surfaces can bounce, spread, and splash, whereas droplets impacting on liquid surfaces can be seen to bounce, coalesce, and splash. The following section discusses the phenomena based on the outcome of impact, nonpenetrative versus penetrative (Figure 3), and the use of droplets to fabricate substrates with heterogeneous wettability.

3. Droplet–substrate interaction

3.1. Droplet impacting into penetrative substrate

Neumann's law establishes the contact angle between a liquid surface drop and a droplet in a quasistatic or steady state[61,62]. The relative difference in surface tension between the droplet and the pool determines the flow pattern and
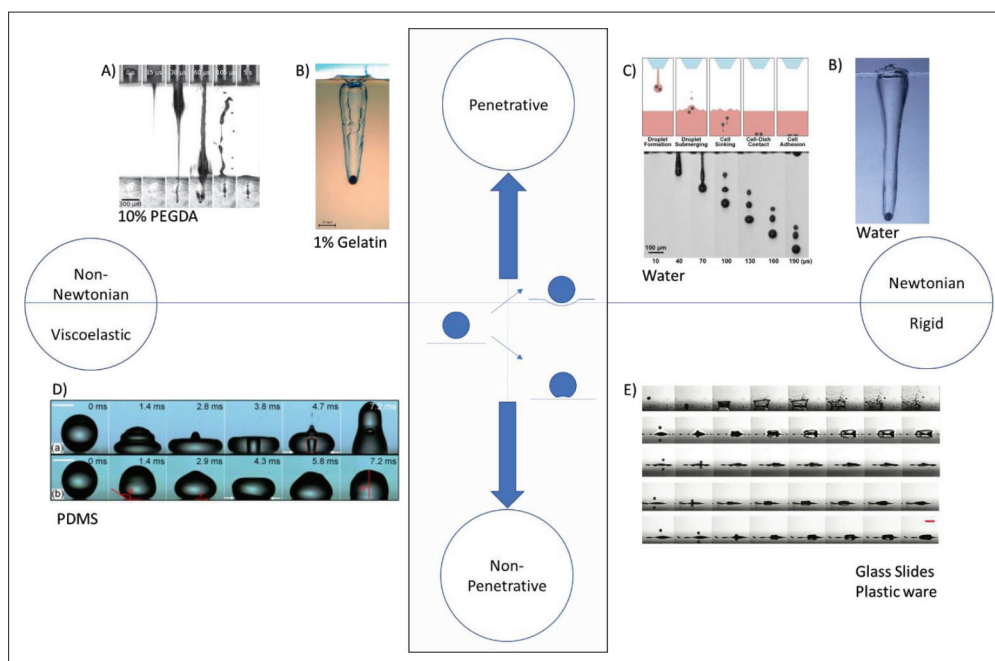
Figure 3. Droplet–substrate interaction classified based on the penetrative and nonpenetrative impact. The penetrative impact on non-Newtonian materials such as PEGDA[56] and gelatin[57]; penetrative impact on Newtonian material such as cell media[58] and water[57]. Nonpenetrative impact on viscoelastic substrate such as PDMS[59], and rigid materials such as glass slides and plasticware[60]. Figures are reproduced under the terms of the Creative Commons Attribution 4.0 International License.

direction of forces. The surface flow is driven inward, and the droplet is injected deep into the pool when the droplet's surface tension is greater than that of the pool. On the other hand, the droplet spreads across the pool surface when the surface tension is lower. The droplet may penetrate the pool if it has the same surface tension as the water. Inhibiting direct contact and coalescence between droplet and receiving substrate results in droplet bouncing on miscible/same liquid[63].

Droplet impact on another liquid surface may result in floating, bouncing, coalescence, or splashing, as described in a previous study and demonstrated in Figure 4[64]. A floating drop will usually disappear after a few seconds into the liquid. Bouncing of the droplet can occur when the impact velocity and the size of a single droplet is small enough[65]. If floating or bouncing of the droplet did not occur post collision, the impact will result in coalescence or splashing. Coalescence of the droplet in the liquid can be partial or full. In partial coalescence, some of the droplets merge into the liquid before "pinch off" occurs, where a secondary droplet is created and bounces off the surface just like splashing. A critical Ohnesorge number determines where partial and full coalescence phase boundaries lie, $Oh^* = 0.026 \pm 0.001$, while weakly associated with Bond number, $Bo = \frac{g\rho D^2}{\sigma}$ [66].

Splashing produced by drop impact on liquid is distinguished from splashing caused by droplet contact

on solid surfaces through the formation of jet based on the impact[65]. The transition between the coalescence and splashing can be predicted using a combination of Weber number and Froude number, $Fr = \frac{V^2 gD}{\sigma}$. The transition from coalescence to short thick jet occurs when $We = 34.7\, Fr^{0.145}$[67]. The lower limit for large bubble entrapment zone with short thin jet is $We = 41.3\, Fr^{0.179}$[68]. This shift into the small bubble entrapment zone with long thin jet occurs at $We = 48.3\, Fr^{0.247}$. Upper limit for small bubble entrapment is $We = 63.1\, Fr^{0.257}$, in which splashing with long thick jet happens without bubbles[69].

The velocity at which a droplet penetrates into the liquid is weakly dependent on the liquid's viscosity[70]. This is due to the air film that exists between the droplet and the liquid, which primarily serves to cushion droplet penetration into the liquid. From conservation of energy, the penetration velocity is both calculated and experimentally verified to be roughly half of the droplet impact velocity by Tran *et al.*[70]. The penetration depth of a droplet impact into liquid, *h*, is proportional to $\sqrt{We}$ [71]. In the case of bioprinting, a droplet contains particles, such as cells, which are jetted onto a receiving substrate. When Park *et al.*[58] injected cell-laden droplets into a well containing cell culture media, they noticed that the cells sank to the bottom and attached to the liquid-filled substrate.

In tissue engineering and bioprinting, hydrogel is frequently employed as a carrier or substrate material for
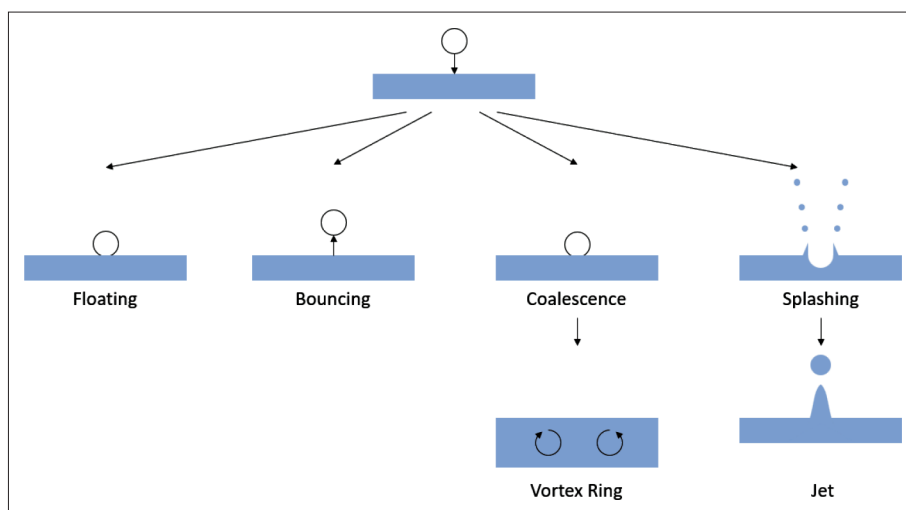
Figure 4. Result of droplet impact on liquid surface.

transferring cells[21,72,73]. Due to their hydrophilic properties resembling biological tissue, hydrogels are polymeric materials that have found extensive use in drug delivery systems[74], implants, and tissue engineering[75,76]. The state of hydrogel is dynamic with its sol–gel transition elicited by interactions such as covalent and noncovalent bonding, electrostatic interaction, temperature, pH changes, ionicity, oxidation state, and enzyme addition[77,78]. Since hydrogel is comprised mainly of water, it may seem natural that water should spread on this substrate as it is soft and permeable. Water droplets, on the other hand, have a nonzero contact angle with a hydrogel surface due to the presence of free polymer chains at the gel interface[79]. It has been observed that the interaction between sessile droplet and the hydrogel surface develop a contact line that exhibits both pinned and receding regimes.

According to Kajiya *et al.*[80], a droplet would initially display a pinned contact line. As a result of the solvent diffusing into the hydrogel below, the contact angle between the liquid and the hydrogel is reduced while the slope of the hydrogel's surface close to the contact line increases. The contact line will recede and balance when the contact angles are almost equal. The diffusion of water into the polymeric surface, which causes the hydrogel to swell, can be used to explain how a surface gradient or slope forms close to the contact angle[80].

Impact work with viscoelastic substrate has been conducted using solid spheres such as silica[81], copper substrate[57], and steel[82]. In general, the elasticity of a substrate influences the cavity formation when a projectile strikes a viscoelastic substrate, such as gelatin. Gelatin, a viscoelastic material, is often used as an analogous material for understanding a ballistic projectile. When studying the projectile of a copper sphere impacting gelatin with varying

concentrations, the sphere either rebounds or penetrates the gelatin substrate depending on concentration[57]. The projectile striking the substrate causes a fracture in both situations.

An example of a liquid projectile penetrating a viscoelastic substrate occurs during jet injection as shown in needleless drug delivery models[56,83,84]. The main determinant of whether a projectile is penetrative or not is whether the jet velocity exceeds a critical value. As described by Park *et al.*[85], jet injection consists of three phases: jet impingement, flow into skin, and dispersion under skin. The jet creates a hole on the viscoelastic substrate when impact pressure is greater than the strength of substrate. For a typical skin strength of 20 MPa, velocity of projectile $v_p \sim 15$ m/s is sufficient to create an impact on the skin[85-87]. The depth of the jet's penetration is determined by the Young's modulus, critical stress for failure, fracture toughness, and hardness of the substrate, such as skin and its equivalents.

The kind of laser, the energy of the laser pulse, and the capillary width all affect the jet power and velocity for optical-based jetting systems. Continuous wave lasers deliver jet in the range of 20–100 m/s, while jet velocity of pulsed lasers are higher and in ranges from 100 to 300 m/s[84]. Mechanical and electromechanical inputs such as spring (100–150 m/s), compressed gas (100–400 m/s), and piezoelectric (20–400 m/s) have been explored as energy sources for jetting[84]. Comparatively, droplet velocity from inkjet technology ranges from 1 to 20 m/s, depending on the composition of ink and types of actuating system[60,88].

Impact velocity, with relative to the substrate, mainly determines the outcome whether the projectile is penetrative or nonpenetrative as demonstrated in the

needleless drug delivery system. The goal in needleless drug delivery is to have targeted drug delivery with certain penetration depth. Leveraging on the rapid firing rate in jet systems, small-volume drugs are delivered into deeper depth using repetitive jetting[56]. Hydrogels, such as gelatin and agarose, have been used in these studies to simulate stiffness of human skin tissue. Similarly, hydrogel has been widely used in bioprinting as both the ink formulation and receiving substrate. There is limited understanding of droplet impact by jetting at the sol–gel transition of hydrogel, as most ballistic studies are conducted on crosslinked hydrogel surfaces or using solid spheres, which does not translate to the viscoelastic nature of cells and cell-laden hydrogel.

3.2. Droplet impacting on nonpenetrative substrate

Jetted droplet formation dissipates kinetic energy upon impacting a surface. Surface energy interaction of the jetted droplet with its substrate influences the spreading morphology of droplet on the nonpenetrative surface. A high-speed droplet impacting on a solid substrate undergoes three phases: (i) rapid spread along the substrate, (ii) take-off from the surface to create the beginning of splash, and (iii) splashing and fragmenting into satellite droplets.

Factors, such as droplet rheology, droplet size, and impact velocity, affect the droplet impact on a substrate[54]. The drop height, air resistance, and ink viscosity have an impact on the droplet's impact velocity[54,89]. Aerodynamic effects are typically disregarded in the inkjet printing process due to the short drop distance (1 mm) between the printing nozzle and the receiving substrate[90]. Thus, inertial force and capillary force, as represented by the Weber number ($We = \frac{\rho v_p^2 d_0}{\sigma}$, where ρ is the density of the fluid, v_p is its impact velocity, d_0 is the droplet diameter, and σ is the surface tension) best describe the behavior of droplet impact. Weber number will typically be higher for high-velocity droplet with large diameter, which implies that the droplet is experiencing higher inertial force than the capillary force. Low-velocity droplets ($We < 5$) will generally adhere to the substrate upon impact, whereas droplets with $5 < We < 10$ usually rebound from a substrate that is smooth and hydrophobic. In other words, the rebound is also the result of a surface characteristic, such as wettability or roughness. The mode of droplet impact upon nonpenetrative substrate is summarized in Table 1[91].

When a droplet impacts the surface with no splashing or rebounding, the droplet will spread across the surface until its maximum drop radius is reached[90]. Thereafter, the drop will either recede from its maximum radius to form a smaller drop or maintain its drop radius. The differences between the cases are dependent on the

Table 1. Classifying different modes of drop impact based on We

Mode of droplet impact	Criteria
Stick	$We < 5$
Rebound	$5 < We < 10$
Spread	$5 < We < 18.0^2 d_0 \left(\frac{\rho}{\sigma}\right)^{0.5} v^{0.25} f^{0.75}$
Splash	$We > 18.0^2 d_0 \left(\frac{\rho}{\sigma}\right)^{0.5} v^{0.25} f^{0.75}$

surface property of the substrate. The maximum spreading droplet diameter, D_{max}, and the initial droplet diameter, D_0, are used to calculate the spreading ratio $\beta = \frac{D_{max}}{D_0}$. The maximum diameter is a balance between inertial forces with capillary and viscous forces. Various models have suggested the relation $\frac{D_{max}}{D_0} = f(Re, We)$, in which Laan et al.[92] suggested the interpolation of two scaling models between the capillary regime (for small We, $\frac{D_{max}}{D_0} \propto We^{\frac{1}{2}}$, and viscous regime (for small Re, $\frac{D_{max}}{D_0} \propto Re^{\frac{1}{5}}$. Generally, high-speed droplet will cause splashing[93]. In comparison to the buoyancy force and stirring force caused by the striking droplet, the surface tension force may produce the strongest flow.

Postimpact, nonpenetrative droplets pin onto the surface with its contact line described by Young's law on surface energies. The spreading and retraction behavior of impact droplets on nonpenetrative viscoelastic substrate is dependent on elasticity of substrate[94]. The dynamic wettability of soft viscoelastic surfaces, such as PDMS, affects the damping coefficient of sessile drop[59,94]. Similar to PDMS surfaces, many natural and synthetic biomaterials exist as soft and deformable films/fibers. Differences between the rigidity and permeability of surfaces influence the droplet–substrate interaction.

For substrates consisting of soft materials, Young's law, which determines the surface energy and contact angle, is no longer valid. Surface tension of the liquid, the stiffness of the material, and the apparent contact angle of the droplet together affect how significantly the contact line between the sessile droplet as well as the elastomeric substrate deforms[95]. The FEM simulation by Tirella et al.[96] showed an inverse effect on substrate stiffness in absorbing the strain energy, which in turns influences droplet remodeling.

Prompt splash occurs when the inertial forces of the droplet overcome the capillary effect of the surface[97]. This phenomena can be simplified and predicted by a "splashing parameter"[98], defined as $K_c = A \cdot Oh^a \cdot We^b$. There are many studies done for the value of A, a, and b at various

Table 2. Summary of splashing parameter for dry or wet solid surface in literature

$K_c = A.\ Oh^a.\ We^b$			Boundary condition	Comment	References
A	**a**	**b**			
1	−0.37	1	Dry surface with different roughness condition	K_c is dependent on roughness. Cossali *et al.*[100] suggested $K_c = 649 + 3.76\ R_{ND}^{-0.63}$, where R_{ND} is the nondimensional roughness defined as R_a/D.	[98]
1	−0.4	1	Wetted surface with different roughness	$K_c = 658$, this splashing parameter is independent of roughness due to the existence of liquid film as explained by Mundo *et al.*[100]	[101]
1	−0.4	1	Wetted surface with different roughness	$K_c = 2100 + 5880\ \delta^{1.44}$, where δ is the nondimensional film thickness defined as h/D, with h being the thickness of liquid layer. The splashing parameter is experimented within $0.1 < \delta < 1.0$	[99]
1	−0.17	0.59	Thin liquid film covering a solid surface	$K_c = 63 = Oh.\ Re^{1.17} \approx \sqrt{We}$, where $\delta = 0.1$	[102]

conditions, such as varying velocity, impact angle, surface roughness, and liquid film thickness. The value is relevant to inkjet bioprinting during the prewetting phase when depositing materials of the first few layers. These scenarios are summarized in Table 2.

In bioprinting, cell compatibility is a major consideration when choosing the appropriate printing technology and formulating bioink for printing. For instance, in droplet-based printing, the splashing of droplet onto substrate has direct impact on cell viability in cell-laden droplet. Ng *et al.*[60] demonstrated the inverse relationship between droplet impact velocity and cell viability. A decrease in droplet impact velocity of cell-laden droplets increases cell viability when jetted against solid surface such as glass slide or petri dishes. The group used HP D300e Digital Dispenser to deposit cell-laden droplet with varying cell concentrations. The HP D300e, a thermal inkjet (TIJ) system, works by vaporizing a small amount of fluid through rapid heating and subsequent generation of a gas bubble that expands to eject precise amounts of fluid. When jetting cells are suspended in a fluid, a higher concentration of cells reduces the splashing of pool from subsequent droplets.

Nooranidoost *et al.*[103] investigated the impact of a cell-laden droplet on a surface to understand the effect of the droplet impingement and droplet spreading on cell viability. The authors determined that the accumulation of stress within the droplet upon impacts deformed cells within the droplet. Additionally, this simulation study demonstrated how enhancing bioink viscoelasticity enhances cell survival by lowering cell deformation during the impact phase. In droplet-based printing methods like inkjet bioprinting, it is advised to employ strategies that lessen cell deformation during and after the jetting and impacting phase of cell-laden droplets.

Another process-specific consideration for droplet-jetting printing processes, such as inkjet printing and aerosol jet printing, lies in the evaporation dynamics of pico- to nanoliter droplets. The evaporation dynamics of the ink influences the pattern of deposition, therefore determining the functionality of ink. A sessile drop's evaporation is complex, which is influenced by a number of variables, including the ink properties (e.g., concentration, additives, particle morphology)[104], substrate properties (e.g., surface roughness, rigidity, permeability, hydrophobicity, texture)[105-108], and the ambient conditions (e.g., humidity and temperature). Higher evaporation kinetics are associated with higher printing resolution, which is determined by smaller droplet size. Other factors that influence print resolution include wettability of surface[109] and suppression of coffee ring effect[110]. Whereas it was found that the droplet would lose volume owing to penetration of liquid into porous and permeable substrate, which occurs faster than evaporation[111]. Substrate wettability increases the infiltration rate, which further suppresses the coffee ring effect by dominating convective flow[111,112]. In inkjet bioprinting, this relation between print resolution and droplet size causes challenge for printing sensitive materials, such as cell-laden ink. In bioprinting, the evaporation dynamics of nanoliter droplets negatively affect cell viability of the cell-laden bioink. There is a trade-off between achieving higher printing resolution and reducing cell viability due to droplet evaporation[60].

3.3. Heterogeneous droplet patterning of substrate

In recent years, researchers are also looking into the droplet impingement behavior on surface with heterogeneous wettability[114,115]. Heterogeneous wettability is created by chemical alteration and physical engineering, giving rise to nonuniformity in adhesion forces along the surface[116]. Unlike dropping on surface with homogenous wettability, the droplets that fall on surface with heterogeneous wettability can experience a resultant lateral force that pushes them sideway because of the asymmetrical force distribution around the droplet caused by the different surface wettability[117]. Generally, the droplets can
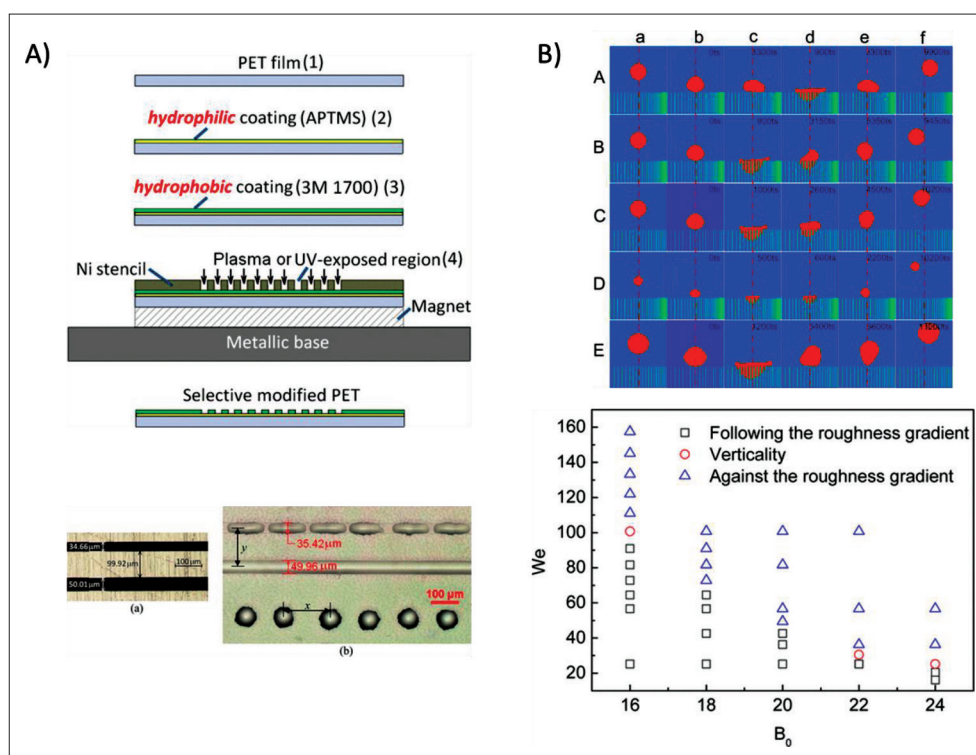
Figure 5. Heterogeneous wettability substrate (A) which influenced the morphology and resolution of ink-jetted droplets (Reprinted with permission from[109]. Copyright (2014) American Chemical Society) and (B) bounce trajectory of droplet impact on penetrative substrate (Reprinted with permission from[113]. Copyright (2016) American Chemical Society).

undergo asymmetric spreading, retracting, detaching, and migrating phases when it impacts on a nonpenetrating surface with a wettability difference and tends to be pushed toward the more hydrophilic area[118]. The high wettability contrast can also result in stronger lateral rebounding force that leads to longer landing distance of the rebounded droplets[119]. However, a different behavior has been observed for penetrable surfaces with wettability difference as Zhang *et al.* have shown that the droplets can move in both directions on a penetrable surface with wettability gradient[113]. The competition between the recoil of droplet on the surface and the penetration of droplet advancing into the groove defines the bounce trajectory. Understanding the trajectory of droplet impact on diverse surfaces may help with the construction of complex engineered tissue as multimaterial 3D bioprinting and integration of various bioprinting and biofabrication modalities advance[120,121].

4. Inkjet for biological applications

Spatial control of biological materials, such as cells, biomaterials, and biological factors, is provided by the inkjet printing system[122]. Interfacial properties of surfaces, such as adhesion, wetting, and opacity, can be tuned to introduce heterogeneity to the substrate[79]. This opens up

new possibilities for creating platforms for biochemical and biophysical research. For instance, pharmacological testing has frequently utilized cell-based high-throughput microarrays.

Droplet size of jetted material influences the number of cells per printed spot, which has been used for creating microarrays of cells with controlled cell density. A single-cell microarray was fabricated using inkjet printing as a proof-of-concept platform for assessing pharmacological treatment[123]. Thin layer of chitosan film with thickness of 70–80 nm was formed when jetted droplets coalesced onto a surface-treated glass substrate with higher hydrophilicity. Then, to create the nonadhesive and adhesive domains on the glass substrate, poly(ethylene glycol) (PEG) and collagen droplets were patterned onto the dried chitosan film, respectively. Cells are seen at spots with collagen droplets when subsequently seeded onto the chitosan/PEG/collagen film. Spot diameter of cell-adhesive material was controlled based on the volume, which correlates to the number of cells found in each spot. Park *et al.*[58] leveraged on the pixelation of inkjet printing and printed graduated concentration of cells. The team demonstrated the concept of pixelation akin to a desktop printer with RGB ink cartridge and patterned different ratio of 3 RGB-labeled cells, giving rise to a heterotypic co-culture model
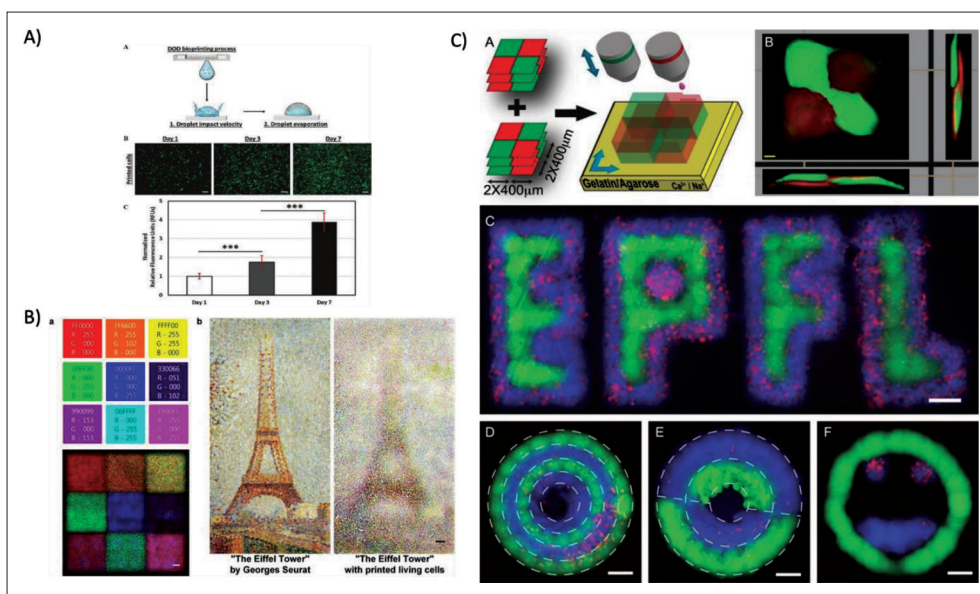
Figure 6. Inkjet printing of cells. (A) Viability of human dermal fibroblast printed through profiling cell proliferation over 7 days[60]. Reproduced under the terms of the Creative Commons Attribution 4.0 International License. (B) Heterogeneous patterning of cell population within region of interest forming color variation similar to home-based inkjet printers[58]. Reproduced under the terms of the Creative Commons Attribution 4.0 International License. (C) Layers of cells patterned with vertical variation[124]. Reproduced under the terms of the Creative Commons Attribution 4.0 International License.

for drug response assays. Negro et al.[124] demonstrated the capability to control heterogeneity in the z-layers by printing several layers of cell-laden hydrogel. Examples above showed that heterogeneous inkjet printing of biomaterials, biomolecules, and cells of different geometries has potential uses in high-throughput drug screening and designing complex tissue structures.

Designing biomaterials with biochemical and mechanical gradients is important for studying cell-material interaction. A platform for studying such interaction should be capable of reproducing this heterogeneity in a reproducible manner. Phillippi used inkjet technology to control the distribution of biochemical cues, thereby inducing multilineage differentiation of stem cells[125]. In this fabrication process, a single source of autologous adult stem cells can be introduced to simultaneously regenerate heterogeneous tissue types using a platform patterned with different growth factors. Biomechanical cues influence cell behavior in the process known as mechanotransduction, where mechanical stimuli are transferred into chemical or electrical signal. Cells are known to react differentially to various mechanical stimulations. This is shown in cell behavioral experiments that demonstrate how MSCs differentiate into neurogenic, myogenic, and osteogenic cells based on the change of the matrix stiffness from soft to stiff to rigid, respectively[126]. Epithelial-metastatic transition (EMT), a crucial biological program involved in embryogenesis, wound healing, cancer cell migration, and metastasis, is yet another illustration[127]. Tuning microenvironment is essential for studying

biological events in cancer progression, wound healing, and embryogenesis[128].

Other than patterning cells and biochemical agents in planar layers, researchers have developed printing strategies to improve shape fidelity of inkjet-printed constructs. One approach is to use a support bath containing crosslinking agents that react with bioink[129-131]. Multicompartment and multicellular structures can be created through leveraging pixelation in inkjet printing technology, as well as the integration of several manufacturing methods (also known as hybrid bioprinting)[132-134]. In the work by Yoon et al.[130], crosslinking agents were spray-coated before each printing layer. The bioink is a modified gelatin-based bioink containing alginate, which reacts with the spray-coated layer of calcium chloride, forming a 3D laminated structure.

Inkjet printing has been applied in planar 2D patterning of cells and biomaterials and constructing 3D tissue constructs for biological application. This is possible through formulating jettable bioinks and designing printing strategies compatible with inkjet technologies. Moving forward, biological functionality of bioprinted constructs is an important criterion in determining the efficacy of bioprinted tissue.

5. Conclusion

From the perspective of material jetting technology in bioprinting, we have a limited understanding of

the substrate–material interaction for non-Newtonian materials like cell-laden polymeric systems. In the case of cell-laden hydrogels, which are commonly used to deliver and deposit materials in bioprinting, increasing our understanding of how jetted droplets interact with different receiving substrates is essential to understanding the impact phase of jetting processes. The concept of hybrid bioprinting, which combines the use of multiple fabrication processes, adds value to bioprinted construct by improving its structural integrity and biological function. The key to integrating different manufacturing technologies lies in understanding material interactions to leverage the distinct advantages of each biomanufacturing process and introduce increased form and functionality to bioprinted constructs.

Acknowledgments

Funding

Conflict of interest

The authors declare no conflict of interests.

Author contributions

Conceptualization: Jia Min Lee
Writing – original draft: Jia Min Lee, Xi Huang, Guo Liang Goh
Writing – review & editing: Jia Min Lee, Tuan Tran, Wai Yee Yeong

Ethics approval and consent to participate

Not applicable.

Consent for publication

Not applicable.

Availability of data

Not applicable.

Further disclosure

Part of or the entire set of findings has been presented in a conference, academic meeting, congress, etc.

References

1. Mir TA, Iwanaga S, Kurooka T, *et al.*, 2019, Biofabrication offers future hope for tackling various obstacles and challenges in tissue engineering and regenerative medicine: A perspective. *Int J Bioprint,* 5(1):153–163.

2. Liu F, *et al.*, 2018, Progress in organ 3D bioprinting. *Int J Bioprint,* 4(1):128–142.

3. Ng WL, Yeong WY, 2019, The future of skin toxicology testing—Three-dimensional bioprinting meets microfluidics. *Int J Bioprint,* 5(2.1):237.

4. Jang T-S, Jung H-D, Pan MH, *et al.*, 2018, 3D printing of hydrogel composite systems: Recent advances in technology for tissue engineering. *Int J Bioprint*, 4(1):126–153.

5. Lee JM, Yeong WY, 2018, Data processing for multi-material 3d bioprinting, in C.K. Chua, W.Y. Yeong, M.J. *et al.*, Eds., in *Proceedings of the 3rd International Conference on Progress in Additive Manufacturing*, 164–169,

   https://doi.org/10.25341/d4x599. [Online]. Available: <Go to ISI>://WOS:000485804300026

6. Ng WL, Chan A, Ong YS, *et al.*, 2020, Deep learning for fabrication and maturation of 3D bioprinted tissues and organs. *Virtual Phys Prototyp*.

   https://doi.org/10.1080/17452759.2020.1771741

7. Ng WL, Lee JM, Zhou M, *et al.*, 2020, Hydrogels for 3-D bioprinting-based tissue engineering, in *Rapid Prototyping of Biomaterials*, R. Narayan Ed. Chapel Hill, NC: Elsevier, 183–204.

8. Gardan J, 2019, Smart materials in additive manufacturing: State of the art and trends. *Virtual Phys Prototyp,* 14(1):1–18.

9. Lee JM, Sing SL, Zhou M, *et al.*, 2018, 3D bioprinting processes: A perspective on classification and terminology. *Int J Bioprint,* 4(2):151.

   https://doi.org/10.18063/ijb.v4i2.151

10. Ahn S, Lee H, Kim G, 2013, Functional cell-laden alginate scaffolds consisting of core/shell struts for tissue regeneration. *Carbohydr Polym,* 98(1):936–942.

    https://doi.org/10.1016/j.carbpol.2013.07.008

11. Billiet T, Gevaert E, De Schryver T, *et al.*, 2014, The 3D printing of gelatin methacrylamide cell-laden tissue-engineered constructs with high cell viability. *Biomaterials,* 35(1):49–62.

    https://doi.org/10.1016/j.biomaterials.2013.09.078

12. Duan B, Hockaday LA, Kang KH, *et al.*, 2013, 3D bioprinting of heterogeneous aortic valve conduits with alginate/gelatin hydrogels. *J Biomed Mater Res Part A,* 101(5):1255–1264.

    https://doi.org/10.1002/jbm.a.34420

13. Fedorovich NE, Wijnberg HM, Dhert WJ, *et al.*, 2011, Distinct tissue formation by heterogeneous printing of

osteo- and endothelial progenitor cells. *Tissue Eng Part A,* 17(15–16):2113–2121.

https//doi.org/10.1089/ten.TEA.2011.0019

14. Huang Y, He K, Wang X, 2013, Rapid prototyping of a hybrid hierarchical polyurethane-cell/hydrogel construct for regenerative medicine. *Mater Sci Eng C,* 33(6):3220–3229.

https//doi.org/10.1016/j.msec.2013.03.048

15. Lee H, Ahn S, Bonassar LJ, *et al.*, 2013, Cell-laden poly(varepsilon-caprolactone)/alginate hybrid scaffolds fabricated by an aerosol cross-linking process for obtaining homogeneous cell distribution: Fabrication, seeding efficiency, and cell proliferation and distribution. *Tissue Eng Part C Methods,* 19(10):784–793.

https//doi.org/10.1089/ten.TEC.2012.0651

16. Ozbolat IT, Chen H, Yu Y, 2014, Development of 'Multi-arm Bioprinter' for hybrid biofabrication of tissue engineering constructs. *Robot Comput Integr Manuf,* 30(3):295–304.

https//doi.org/10.1016/j.rcim.2013.10.005

17. Shim J-H, Lee J-S, Kim JY, *et al.*, 2012, Bioprinting of a mechanically enhanced three-dimensional dual cell-laden construct for osteochondral tissue engineering using a multi-head tissue/organ building system. *J Micromech Microeng,* 22(8):085014.

https//doi.org/10.1088/0960-1317/22/8/085014

18. Snyder JE, Hamid Q, Wang C, *et al.*, 2011, Bioprinting cell-laden matrigel for radioprotection study of liver by pro-drug conversion in a dual-tissue microfluidic chip. *Biofabrication,* 3(3):034112.

https//doi.org/10.1088/1758-5082/3/3/034112

19. Wang X, Yan Y, Pan Y, *et al.*, 2006, Generation of three-dimensional hepatocyte/gelatin structures with rapid prototyping system (in English). *Tissue Eng,* 12(1):83–90.

https//doi.org/DOI 10.1089/ten.2006.12.83

20. Zhuang P, Ng WL, An J, *et al.*, 2019, Layer-by-layer ultraviolet assisted extrusion-based (UAE) bioprinting of hydrogel constructs with high aspect ratio for soft tissue engineering applications. *PLoS One,* 14(6):e0216776.

https//doi.org/10.1371/journal.pone.0216776

21. Lee JM, Yeong WY, 2020, Engineering macroscale cell alignment through coordinated toolpath design using support-assisted 3D bioprinting. *J R Soc Interface*, 17(168):20200294.

https//doi.org/doi:10.1098/rsif.2020.0294

22. Skardal A, Zhang J, Prestwich GD, 2010, Bioprinting vessel-like constructs using hyaluronan hydrogels crosslinked with tetrahedral polyethylene glycol tetracrylates. *Biomaterials*, 31(24):6173–6181.

https//doi.org/10.1016/j.biomaterials.2010.04.045

23. Visser J, Peters B, Burger TJ, *et al.*, 2013, Biofabrication of multi-material anatomically shaped tissue constructs. *Biofabrication,* 5(3):035007.

https//doi.org/10.1088/1758-5082/5/3/035007

24. Ng WL, Yeong WY, Naing MW, 2016, Microvalve bioprinting of cellular droplets with high resolution and consistency. *Proceedings of the International Conference on Progress in Additive Manufacturing.* 397–402.

https//doi.org/10.3850/2424-8967_V02-236

25. Ng WL, Lee JM, Yeong WY, *et al.*, 2017, Microvalve-based bioprinting—Process, bio-inks and applications. *Biomater Sci,* 5(4):632–647.

26. Masaeli E, Forster V, Picaud S, *et al.*, 2020, Tissue engineering of retina through high resolution 3-dimensional inkjet bioprinting. *Biofabrication,* 12(2): Art no. 025006.

https//doi.org/10.1088/1758-5090/ab4a20

27. Solis LH, Ayala Y, Portillo S, *et al.*, 2019, Thermal inkjet bioprinting triggers the activation of the VEGF pathway in human microvascular endothelial cells in vitro. *Biofabrication,* 11(4): Art no. 045005.

https//doi.org/10.1088/1758-5090/ab25f9

28. Angelopoulos I, Allenby MC, Lim M, *et al.*, 2020, Engineering inkjet bioprinting processes toward translational therapies. *Biotechnol Bioeng,* 117(1):272–284.

https//doi.org/10.1002/bit.27176

29. Wu DZ, Xu CX, 2018, Predictive modeling of droplet formation processes in inkjet-based bioprinting. *J Manuf Sci Eng Transact Asme,* 140(10): Art no. 101007.

https//doi.org/10.1115/1.4040619

30. Guillemot F, Guillotin B, Fontaine A, *et al.*, 2011, Laser-assisted bioprinting to deal with tissue complexity in regenerative medicine (in English). *Mrs Bull,* 36(12): 1015–1019.

https//doi.org/Doi 10.1557/Mrs.2011.272

31. Guillotin B, Souquet A, Catros S, *et al.*, 2010, Laser assisted bioprinting of engineered tissue with high cell density and microscale organization. *Biomaterials*, 31(28):7250–7256.

32. Gruene M, Deiwick A, Koch L, *et al.*, 2011, Laser printing of stem cells for biofabrication of scaffold-free autologous grafts. *Tissue Eng Part C Methods,* 17(1):79–87.

https//doi.org/10.1089/ten.tec.2010.0359

33. Guillemot F, Souquet A, Catros S, *et al.*, 2010, High-throughput laser printing of cells and biomaterials for tissue engineering. *Acta Biomater,* 6(7):2494–2500.

https//doi.org/10.1016/j.actbio.2009.09.029

34. Ng WL, Lee JM, Zhou M, *et al.*, 2020, Vat polymerization-based bioprinting–process, materials, applications and regulatory challenges. *Biofabrication,* 12(2):022001.

https//doi.org/10.1088/1758-5090/ab6034

35. Soman P, Chung H, Zhang AP, *et al.*, 2013, Digital microfabrication of user-defined 3D microstructures in cell-laden hydrogels (in English). *Biotechnol Bioeng*, 110(11):3038–3047.

https//doi.org/Doi 10.1002/Bit.24957

36. Zhu W, Qu X, Zhu J, *et al.*, 2017, Direct 3D bioprinting of prevascularized tissue constructs with complex microarchitecture. *Biomaterials,* 124:106–115.

https//doi.org/10.1016/j.biomaterials.2017.01.042

37. Gauvin R, Chen YC, Lee JW, *et al.*, 2012, Microfabrication of complex porous tissue engineering scaffolds using 3D projection stereolithography. *Biomaterials,* 33(15): 3824–3834.

https//doi.org/10.1016/j.biomaterials.2012.01.048

38. Wang Z, Kumar H, Tian Z, *et al.*, 2018, Visible light photoinitiation of cell-adhesive gelatin methacryloyl hydrogels for stereolithography 3D bioprinting. *ACS Appl Mater Interfaces,* 10(32):26859–26869.

https//doi.org/10.1021/acsami.8b06607

39. Mahdavi SS, Abdekhodaie MJ, Kumar H, *et al.*, 2020, Stereolithography 3D bioprinting method for fabrication of human corneal stroma equivalent. *Ann Biomed Eng,* 48(7):1955–1970.

https//doi.org/10.1007/s10439-020-02537-6

40. Mao Q, Wang Y, Li Y, *et al.*, 2020, Fabrication of liver microtissue with liver decellularized extracellular matrix (dECM) bioink by digital light processing (DLP) bioprinting. *Mater Sci Eng C Mater Biol Appl,* 109: Art no. 110625.

https//doi.org/10.1016/j.msec.2020.110625

41. Gudupati H, Dey M, Ozbolat I, 2016, A comprehensive review on droplet-based bioprinting: Past, present and future. *Biomaterials*, 102:20–42.

42. Li X, Liu B, Pei B, *et al.*, 2020, Inkjet bioprinting of biomaterials. *Chem Rev,* 120(19):10793–10833.

https//doi.org/10.1021/acs.chemrev.0c00008

43. Liu Y, Derby B, 2019, Experimental study of the parameters for stable drop-on-demand inkjet performance. *Phys Fluids,* 31(3):032004.

https//doi.org/10.1063/1.5085868

44. Yan J, Huang Y, Xu C, *et al.*, 2012, Effects of fluid properties and laser fluence on jet formation during laser direct writing of glycerol solution. *J Appl Phys,* 112(8):083105.

https//doi.org/10.1063/1.4759344

45. Kang SH, Kim S, Lim JW, *et al.*, 2020, Study on fall velocity of continuously ejected micro inkjet droplet. *J Mech Sci Technol*, 34(8):3311–3315.

https//doi.org/10.1007/s12206-020-0723-1

46. Xu C, Zhang Z, Fu J, *et al.*, 2017, Study of pinch-off locations during drop-on-demand inkjet printing of viscoelastic alginate solutions. *Langmuir,* 33(20):5037–5045.

https//doi.org/10.1021/acs.langmuir.7b00874

47. Poole R, 2012, The deborah and weissenberg numbers. *Rheol Bull,* 53(2):32–39.

48. Vadillo DC, Tuladhar TR, Mulji AC, *et al.*, 2010, Evaluation of the inkjet fluid's performance using the "Cambridge Trimaster" filament stretch and break-up device. *J Rheol,* 54(2):261–282.

https//doi.org/10.1122/1.3302451

49. Modak CD, Kumar A, Tripathy A, *et al.*, 2020, Drop impact printing. *Nat Commun,* 11(1):4327.

https//doi.org/10.1038/s41467-020-18103-6

50. Meyer JD, Bazilevsky AV, Rozhkov AN, 1997, *Effects of Polymeric Additives on Thermal Ink Jets*, Seattle, WA.

51. Morrison NF, Harlen OG, 2010, Viscoelasticity in inkjet printing. *Rheol Acta,* 49(6):619–632.

https//doi.org/10.1007/s00397-009-0419-z

52. Suly P, Sevcik J, Dmonte DJ, *et al.*, 2021, Inkjet printability assessment of weakly viscoelastic fluid: A semidilute polyvinylpyrrolidone solution ink case study. *Langmuir,* 37(28):8557–8568.

https//doi.org/10.1021/acs.langmuir.1c01010

53. Du Z, Lin Y, Xing R, *et al.*, 2018, Controlling the polymer ink's rheological properties and viscoelasticity to suppress satellite droplets. *Polymer,* 138:75–82.

https//doi.org/10.1016/j.polymer.2018.01.052

54. Jang D, Kim D, Moon J, 2009, Influence of fluid physical properties on ink-jet printability. *Langmuir,* 25(5):2629–2635.

https//doi.org/10.1021/la900059m

55. Blaeser A, Campos DFD, Puster U, *et al.*, 2016, Controlling shear stress in 3D bioprinting is a key factor to balance printing resolution and stem cell integrity. *Adv Healthc Mater,* 5(3):326–333.

https//doi.org/10.1002/adhm.201500677

56. Krizek J, Delrot P, Moser C, 2020, Repetitive regime of highly focused liquid microjets for needle-free injection. *Sci Rep,* 10(1):5067.

https//doi.org/10.1038/s41598-020-61924-0

57. Kiyama A, Mansoor MM, Speirs NB, *et al.*, 2019, Gelatine cavity dynamics of high-speed sphere impact. *J Fluid Mech,* 880:707–722.

https//doi.org/10.1017/jfm.2019.696

58. Park JA, Yoon S, Kwon J, *et al.*, 2017, Freeform micropatterning of living cells into cell culture medium using direct inkjet printing. *Sci Rep*, 7(1):14610.

https//doi.org/10.1038/s41598-017-14726-w

59. Chen L, Bonaccurso E, Deng P, *et al.*, 2016, Droplet impact on soft viscoelastic surfaces. *Phys Rev E*, 94(6):063117.

https//doi.org/10.1103/PhysRevE.94.063117

60. Ng WL, Huang X, Shkolnikov V, *et al.*, 2021, Controlling droplet impact velocity and droplet volume: Key factors to achieving high cell viability in sub-nanoliter droplet-based bioprinting. *Int J Bioprint,* 8(1).

https//doi.org/10.18063/ijb.v8i1.424

61. Andreotti B, Snoeijer JH, 2020, Statics and dynamics of soft wetting. *Ann Rev Fluid Mech,* 52(1):285–308.

https//doi.org/10.1146/annurev-fluid-010719-060147

62. Aljedaani AB, Wang C, Jetly A, *et al.*, 2018, Experiments on the breakup of drop-impact crowns by Marangoni holes. *J Fluid Mech,* 844:162–186.

https//doi.org/10.1017/jfm.2018.178

63. Han X, Li J, Tang X, *et al.*, 2022, Droplet bouncing: Fundamentals, regulations, and applications. *Small,* 18(22):2200277.

https://doi.org/10.1002/smll.202200277.

64. Rein M, 1993, Phenomena of liquid drop impact on solid and liquid surfaces. *Fluid Dynamics Res,* 12(2):61–93.

65. Rodriguez F, Mesler R, 1985, Some drops don't splash. *J Colloid Interface Sci,* 106(2):347–352.

https://doi.org/10.1016/S0021-9797(85)80008-4

66. Blanchette F, Bigioni TP, 2006, Partial coalescence of drops at liquid interfaces. *Nat Phys,* 2(4):254–257.

67. Rodriguez F, Mesler R, 1988, The penetration of drop-formed vortex rings into pools of liquid. *J Colloid Interface Sci,* 121(1):121–129.

https://doi.org/10.1016/0021-9797(88)90414-6

68. Oguz HN, Prosperetti A, 1990, Bubble entrainment by the impact of drops on liquid surfaces. *J Fluid Mech,* 219: 143–179.

https//doi.org/10.1017/S0022112090002890

69. Ray B, Biswas G, Sharma A, 2015, Regimes during liquid drop impact on a liquid pool. *J Fluid Mech,* 768:492–523.

https//doi.org/10.1017/jfm.2015.108

70. Tran T, de Maleprade H, Sun C, *et al.*, 2013, Air entrainment during impact of droplets on liquid surfaces. *J Fluid Mech,* 726:R3, Art no. R3.

https//doi.org/10.1017/jfm.2013.261

71. Gielen MV, Sleutel P, Benschop J, *et al.*, 2017, Oblique drop impact onto a deep liquid pool. *Phys Rev Fluids*, 2(8):083602.

https//doi.org/10.1103/PhysRevFluids.2.083602

72. Lee JM, Yeong WY, 2016, Design and printing strategies in 3D bioprinting of cell-hydrogels: A review. *Adv Healthc Mater,* 5(22):2856–2865.

73. Soetedjo AA, Lee JM, Lau HH, *et al.*, 2021, Tissue engineering and 3D printing of bioartificial pancreas for regenerative medicine in diabetes. *Trends Endocrinol Metab,* 32(8):609–622.

74. Mandal A, Clegg JR, Anselmo AC, *et al.*, 2020, Hydrogels in the clinic (in English). *Bioeng Transl Med,* 5(2):e10158–e10158.

https://doi.org/10.1002/btm2.10158

75. Salg GA, Giese NA, Schenk M, *et al.*, 2019, The emerging field of pancreatic tissue engineering: A systematic review and evidence map of scaffold materials and scaffolding techniques for insulin-secreting cells. *J Tissue Eng,* 10:2041731419884708.

76. Dang TT, Nikkhah M, Memic A, *et al.*, 2014, Chapter 19—Polymeric biomaterials for implantable prostheses, in *Natural and Synthetic Biomedical Polymers*, SG Kumbar, CT Laurencin, M Deng, Eds. Oxford: Elsevier, 309–331.

77. Wang S, Lee JM, Yeong WY, 2015, Smart hydrogels for 3D bioprinting. *Int J Bioprint*, 1(1):12.

https://doi.org/10.18063/ijb.2015.01.005.

78. Nele V, Wojciechowski JP, Armstrong JPK, *et al.*, 2020, Tailoring gelation mechanisms for advanced hydrogel applications. *Adv Funct Mater,* 30(42):2002759.

https://doi.org/10.1002/adfm.202002759

79. Boulogne F, Ingremeau F, Limat L, *et al.*, 2016, Tuning the receding contact angle on hydrogels by addition of particles. *Langmuir*, 32(22):5573–5579.

https://doi.org/10.1021/acs.langmuir.6b01209

80. Kajiya T, Daerr A, Narita T, *et al.*, 2011, Dynamics of the contact line in wetting and diffusing processes of water droplets on hydrogel (PAMPS–PAAM) substrates. *Soft Matter,* 7(24):11425–11432.

81. Veysset D, Kooi SE, Maznev AA, *et al.*, 2018, High-velocity micro-particle impact on gelatin and synthetic hydrogel. *J Mech Behav Biomed Mater,* 86:71–76.

https://doi.org/10.1016/j.jmbbm.2018.06.016

82. Mrozek RA, Leighliter B, Gold CS, *et al.*, 2015, The relationship between mechanical properties and ballistic penetration depth in a viscoelastic gel. *J Mech Behav Biomed Mater,* 44:109–120.

https://doi.org/10.1016/j.jmbbm.2015.01.001

83. Baxter J, Mitragotri S, 2005, Jet-induced skin puncture and its impact on needle-free jet injections: Experimental studies and a predictive model. *J Controll Release,* 106(3):361–373.

https://doi.org/10.1016/j.jconrel.2005.05.023

84. Schoppink J, Fernandez Rivas D, 2022, Jet injectors: Perspectives for small volume delivery with lasers. *Adv Drug Deliv Rev,* 182:114109.

https://doi.org/10.1016/j.addr.2021.114109

85. Park M-a, Jang H-j, Sirotkin FV, *et al.*, 2012, Er:YAG laser pulse for small-dose splashback-free microjet transdermal drug delivery. *Opt Lett,* 37(18):3894–3896.

https//doi.org/10.1364/OL.37.003894

86. Berrospe-Rodriguez C, Visser CW, Schlautmann S, *et al.*, 2016, Continuous-wave laser generated jets for needle free applications. *Biomicrofluidics,* 10(1):014104.

https//doi.org/10.1063/1.4940038

87. Cu K, Bansal R, Mitragotri S, *et al.*, 2020, Delivery strategies for skin: Comparison of nanoliter jets, needles and topical solutions. *Ann Biomed Eng,* 48(7):2028–2039.

https//doi.org/10.1007/s10439-019-02383-1

88. Zhao D, Zhou H, Wang Y, *et al.*, 2021, Drop-on-demand (DOD) inkjet dynamics of printing viscoelastic conductive ink. *Addit Manuf,* 48:102451.

https://doi.org/10.1016/j.addma.2021.102451

89. Wijshoff H, 2018, Drop dynamics in the inkjet printing process. *Curr Opin Colloid Interface Sci,* 36:20–27.

https//doi.org/10.1016/j.cocis.2017.11.004

90. Josserand C, Thoroddsen ST, 2016, Drop impact on a solid surface. *Annu Rev Fluid Mech,* 48:365–391.

91. Stanton DW, Rutland CJ, 1998, Multi-dimensional modeling of thin liquid films and spray-wall interactions resulting from impinging sprays. *Int J Heat Mass Transf,* 41(20): 3037–3054.

92. Laan N, de Bruin KG, Bartolo D, *et al.*, 2014, Maximum diameter of impacting liquid droplets. *Phys Rev Appl,* 2(4):044018.

https//doi.org/10.1103/PhysRevApplied.2.044018

93. Yarin AL, 2006, Drop impact dynamics: Splashing, spreading, receding, bouncing…. *Annu Rev Fluid Mech,* 38:159–192.

94. Alizadeh A, Bahadur V, Shang W, *et al.*, 2013, Influence of substrate elasticity on droplet impact dynamics. *Langmuir,* 29(14):4520–4524.

https//doi.org/10.1021/la304767t

95. Park SJ, Weon BM, Lee JS, *et al.*, 2014, Visualization of asymmetric wetting ridges on soft solids with X-ray microscopy. *Nat Commun,* 5(1):4369.

https//doi.org/10.1038/ncomms5369

96. Tirella A, Vozzi F, De Maria C, *et al.*, 2011, Substrate stiffness influences high resolution printing of living cells with an ink-jet system. *J Biosci Bioeng,* 112(1):79–85.

https//doi.org/10.1016/j.jbiosc.2011.03.019

97. Moreira ALN, Moita AS, Panão MR, 2010, Advances and challenges in explaining fuel spray impingement: How much of single droplet impact research is useful? *Progr Energy Combust Sci,* 36(5):554–580.

https//doi.org/10.1016/j.pecs.2010.01.002

98. Stow CD, Hadfield MG, 1981, An experimental investigation of fluid flow resulting from the impact of a water drop with an unyielding dry surface. *Proc R Soc Lond A Math Phys Sci,* 373(1755):419–441.

99. Cossali GE, Coghe A, Marengo M, 1997, The impact of a single drop on a wetted solid surface. *Exp Fluids,* 22(6): 463–472.

https//doi.org/10.1007/s003480050073

100. Mundo C, Sommerfeld M, Tropea C, 1998, On the modeling of liquid sprays impinging on surfaces. *Atom Sprays,* 8(6): 625–652.

101. Mundo C, Sommerfeld M, Tropea C, 1995, Droplet-wall collisions: Experimental studies of the deformation and breakup process. *Int J Multiphase Flow,* 21(2):151–173.

https//doi.org/10.1016/0301-9322(94)00069-V

102. Wal RLV, Berger GM, Mozes SD, 2006, The splash/non-splash boundary upon a dry surface and thin fluid film. *Exp Fluids,* 40(1):53–59.

https//doi.org/10.1007/s00348-005-0045-1

103. Nooranidoost M, Izbassarov D, Tasoglu S, *et al.*, 2019, A computational study of droplet-based bioprinting: Effects of viscoelasticity. *Phys Fluids,* 31(8):081901.

https//doi.org/10.1063/1.5108824

104. Goh GL, Saengchairat N, Agarwala S, *et al.*, 2019, Sessile droplets containing carbon nanotubes: A study of evaporation dynamics and CNT alignment for printed electronics. *Nanoscale,* 11(22):10603–10614.

105. Nguyen TA, Nguyen AV, Hampton MA, *et al.*, 2012, Theoretical and experimental analysis of droplet evaporation on solid surfaces. *Chem Eng Sci,* 69(1):522–529.

106. Shanahan M, Sefiane K, Moffat J, 2011, Dependence of volatile droplet lifetime on the hydrophobicity of the substrate. *Langmuir,* 27(8):4572–4577.

107. Duursma G, Sefiane K, David S, 2010, Advancing and receding contact lines on patterned structured surfaces. *Chem Eng Res Design,* 88(5-6):737–743.

108. Sefiane K, Wilson S, David S, *et al.*, 2009, On the effect of the atmosphere on the evaporation of sessile droplets of water. *Phys Fluids,* 21(6):062101.

109. Nguyen PQM, Yeo L-P, Lok B-K, *et al.*, 2014, Patterned surface with controllable wettability for inkjet printing of flexible printed electronics. *ACS Appl Mater Interfaces,* 6(6):4011–4016.

https//doi.org/10.1021/am4054546

110. Lee JM, Yeong WY, 2015, A preliminary model of time-pressure dispensing system for bioprinting based on printing and material parameters. *Virtual Phys Prototyp,* 10(1): 3–8.

https//doi.org/10.1080/17452759.2014.979557

111. Pack M, Hu H, Kim D-O, *et al.*, 2015, Colloidal drop deposition on porous substrates: Competition among particle motion, evaporation, and infiltration. *Langmuir,* 31(29):7953–7961.

112. Dou R, Derby B, 2012, Formation of coffee stains on porous surfaces. *Langmuir,* 28(12):5331–5338.

113. Zhang B, Lei Q, Wang Z, *et al.*, 2016, Droplets can rebound toward both directions on textured surfaces with a wettability gradient. *Langmuir,* 32(1):346–351.

114. Zhao J, Chen S, Liu Y, 2017, Dynamical behaviors of droplet impingement and spreading on chemically heterogeneous surfaces. *Appl Surf Sci,* 400:515–523.

115. Clavijo CE, Crockett J, Maynes D, 2017, Hydrodynamics of droplet impingement on hot surfaces of varying wettability. *Int J Heat Mass Transf,* 108:1714–1726.

116. Li H, Li A, Zhao Z, *et al.*, 2020, Heterogeneous wettability surfaces: Principle, construction, and applications. *Small Struct,* 1(2):2000028.

    https://doi.org/10.1002/sstr.202000028

117. Lim C, Lam Y, 2014, An investigation into a micro-sized droplet impinging on a surface with sharp wettability contrast. *J Phys D Appl Phys,* 47(42):425305.

118. Yuan Z, Matsumoto M, Kurose R, 2020, Directional migration of an impinging droplet on a surface with wettability difference. *Phys Rev Fluids,* 5(11):113605.

119. Farshchian B, Pierce J, Beheshti MS, *et al.*, 2018, Droplet impinging behavior on surfaces with wettability contrasts. *Microelectron Eng,* 195:50–56.

120. Lee JM, Sing SL, Yeong WY, 2020, Bioprinting of multimaterials with computer-aided design/computer-aided manufacturing (in English). *Int J Bioprint,* 6(1):245.

    https://doi.org/10.18063/ijb.v6i1.245

121. AlZaid S, Hammad N, Albalawi HI, *et al.*, 2022, Advanced software development of 2D and 3D model visualization for TwinPrint, a dual-arm 3D bioprinting system for multi-material printing. *Mater Sci Addit Manuf,* 1(3):19–25.

    https://doi.org/10.18063/msam.v1i3.19

122. Wang D, Ker DF, Ng KW, *et al.*, 2021, Combinatorial mechanical gradation and growth factor biopatterning strategy for spatially controlled bone-tendon-like cell differentiation and tissue formation. *NPG Asia Mater,* 13(1):26.

    https://doi.org/10.1038/s41427-021-00294-z

123. Ferrara V, Zito G, Arrabito G, *et al.*, 2020, Aqueous processed biopolymer interfaces for single-cell microarrays. *ACS Biomater Sci Eng,* 6(5):3174–3186.

    https://doi.org/10.1021/acsbiomaterials.9b01871

124. Negro A, Cherbuin T, Lutolf MP, 2018, 3D inkjet printing of complex, cell-laden hydrogel structures. *Sci Rep,* 8(1):17099.

    https://doi.org/10.1038/s41598-018-35504-2

125. Phillippi JA, Miller E, Weiss L, *et al.*, 2008, Microenvironments engineered by inkjet bioprinting spatially direct adult stem cells toward muscle- and bone-like subpopulations. *Stem Cells,* 26(1):127–134.

    https://doi.org/10.1634/stemcells.2007-0520

126. Engler AJ, Sen S, Sweeney HL, *et al.*, 2006, Matrix elasticity directs stem cell lineage specification. *Cell,* 126(4): 677–689.

    https://doi.org/10.1016/j.cell.2006.06.044

127. Dongre A, Weinberg RA, 2019, New insights into the mechanisms of epithelial–mesenchymal transition and implications for cancer. *Nat Rev Mol Cell Biol,* 20(2): 69–84.

    https://doi.org/10.1038/s41580-018-0080-4

128. Mihalko EP, Brown AC, 2018, Material strategies for modulating epithelial to mesenchymal transitions. *ACS Biomater Sci Eng,* 4(4):1149–1161.

    https://doi.org/10.1021/acsbiomaterials.6b00751

129. Arai K, Iwanaga S, Toda H, *et al.*, 2011, Three-dimensional inkjet biofabrication based on designed images. *Biofabrication,* 3(3):034113.

130. Yoon S, Park JA, Lee H-R, *et al.*, 2018, Inkjet–spray hybrid printing for 3D freeform fabrication of multilayered hydrogel structures. *Adv Healthc Mater,* 7(14):1800050.

    https://doi.org/10.1002/adhm.201800050

131. Xu T, Zhao W, Zhu J-M, *et al.*, 2013, Complex heterogeneous tissue constructs containing multiple cell types prepared by inkjet printing technology. *Biomaterials,* 34(1):130–139.

132. Agarwala S, Lee JM, Ng WL, *et al.*, 2018, A novel 3D bioprinted flexible and biocompatible hydrogel bioelectronic platform. *Biosens Bioelectron,* 102:365–371.

    https://doi.org/10.1016/j.bios.2017.11.039

133. Lee JM, Sing SL, Zhou M, *et al.*, 2018, 3D bioprinting processes: A perspective on classification and terminology (in English). *Int J Bioprint,* 4(2):151.

    https://doi.org/10.18063/IJB.v4i2.151

134. Lee H-R, Park JA, Kim S, *et al.*, 2021, 3D microextrusion-inkjet hybrid printing of structured human skin equivalents. *Bioprinting,* 22:e00143.

    https://doi.org/10.1016/j.bprint.2021.e00143